International Journal of Legal Medicine
https://doi.org/10.1007/s00414-020-02273-5

METHOD PAPER

Diagnosis of pulmonary infarction in post-mortem computed tomography and post-mortem magnetic resonance imaging—a technical note

Nicolas Herr[1] · Paolo Lombardo[1,2] · Christian Jackowski[1] · Wolf Dieter Zech[1]

Received: 27 March 2019 / Accepted: 12 March 2020

Abstract
Pulmonary thromboembolism may be accompanied by pulmonary infarction. Even though pulmonary thromboembolism (PTE) is a frequently found cause of death at autopsy, pulmonary infarction accompanying PTE is a less common finding and may therefore easily be misinterpreted as infectious or cancerous lung disease. Appearance of pulmonary infarction in post-mortem imaging and acquisition parameters helping to identify pulmonary infarctions are not described yet. Based on a case of a 50-year-old man who died due to PTE and presented pulmonary infarction, we suggest using a pulmonary algorithm in post-mortem computed tomography combined with post-mortem magnetic resonance imaging of the lungs using conventional T1- and T2-weighted sequences.

Keywords Pulmonary infarction · Pulmonary thromboembolism · Post-mortem computed tomography · Post-mortem magnetic resonance imaging

Introduction

We present post-mortem imaging and autopsy results of a 50-year-old man who died from right cardiac failure due to PTE. Post-mortem imaging comprised whole-body unenhanced post-mortem computed tomography (PMCT) and unenhanced post-mortem magnetic resonance (PMMR) imaging of the chest prior to forensic autopsy. PM-imaging revealed pulmonary findings suspicious of pulmonary infarction.

Methods and results

Post-mortem imaging (PMCT and PMMR)

The interval between death and PMCT was 5 h. Whole-body unenhanced PMCT imaging was performed as part of the routine forensic examination using a Siemens Somatom Definition AS 64. Tube voltage was 140 kV, caredose, slice thickness 1 mm, increment 0.7 mm, a rotation time of 0.5 s, and a field of view of 570 mm. Soft tissue algorithm and bone tissue algorithm were used. The thorax was reconstructed using a specific pulmonary algorithm with a field of view of 332 mm.

PMMR of the thorax was conducted immediately after PMCT. Body temperature at the time of scanning was 23 °C. For PMMR (Philips Achiva 3T) imaging, the body was placed in an artifact-free body bag. The applied sequences were T2-weighted sequences (T2_Dixon_tra: slice thickness, 3 mm; GAP, 0.3 mm; TR, 3957 ms; TE, 90 ms; NSA, 2 and T2_Dixon_cor: slice thickness, 3 mm; GAP, 0.3 mm; TR, 3957 ms; TE, 90 ms; NSA, 2) as well as T1-weighted sequences (T1_Dixon_tra: slice thickness, 3 mm; GAP, 0.3 mm; TR, 702 ms; TE, 7.39 ms; NSA, 1 and T1_Dixon_cor: slice thickness, 3 mm; GAP, 0.3 mm; TR, 702 ms; TE, 7.44 ms; NSA, 1). Dixon technique was chosen according to our standard PMMR-protocol allowing to obtain water only, fat only, and in-phase and out-of-phase images in a single acquisition. PMMR examination time was 25 min. All images (PMCT and PMMR) were viewed and evaluated in a PACS (Sectra Workstation IDS7, Version 17.1.16.3569, Linköping/Sweden) by a

✉ Wolf Dieter Zech
wolf-dieter.zech@irm.unibe.ch

[1] Institute of Forensic Medicine, University of Bern, Bühlstrasse 20, 3012 Bern, Switzerland

[2] Department of Diagnostic, Interventional and Pediatric Radiology, University of Bern, Inselspital, Freiburgstrasse 10, 3010 Bern, Switzerland

Published online: 01 April 2020

board-certified radiologist experienced in post-mortem imaging.

Postmortem imaging results

PMCT and PMMR showed three wedge-shaped, pleura-based lesions in the lung periphery (one lesion in the upper right lobe, approx. 29 mm × 22 mm × 31 mm, and two in the lower right lobe, approx. 25 mm × 21.5 mm × 26 mm and 40 mm × 29 mm × 38 mm, respectively). Lesions appeared mainly hyperdense with smaller hypodense areas in PMCT (Fig. 1). In PMMR, lesions appeared mainly hypointense to isointense containing focal hypointense areas in T1w and mainly hyperintense with focal hypointense areas in T2w in-phase images (Fig. 1). Appearance of pulmonary lesions in Dixon water only, fat only, and out-of-phase images is shown in Table 1. Additionally, homogeneous material of intermediate signal intensity within the large and small pulmonary arteries of both lungs compatible with PTE was found in T2w PMMR [1].

Autopsy and histology

Autopsy was conducted immediately after imaging by board-certified forensic pathologists according to the Recommendation of the Committee of Ministers to Member States of Europe on the harmonization of medico-legal autopsy rules [2] and included external and internal examination with opening of all three body cavities and dissection of all organs. During autopsy, tissue samples of the lung as well as tissue samples from all other internal organs were collected for histologic examination. Histology staining included hematoxylin and eosin (H&E) and iron (Fe) staining. Histologic examinations and adjudication were performed by board-certified forensic pathologists. Toxicological examinations were not commissioned by the prosecutor.

Autopsy and histology findings

External examination showed signs of upper venous congestion with livid discoloration of the face, neck, and upper chest as well as a visible engorgement of the jugular veins. Internal examination revealed thromboembolic occlusion of the large and small pulmonary arteries of both lungs, partially attached to the vessel walls. Wedge-shaped lesions seen in PMCT and PMMR in the upper and lower lobe of the right lung periphery were identified as pulmonary infarction with surrounding hemorrhage.

H&E staining of the wedge-shaped lung lesions showed central infarcted necrotic lung tissue and a surrounding hemorrhagic rim. Iron staining revealed iron-positive macrophages at the edge of necrotic lung tissue.

Furthermore, autopsy showed concentric hypertrophy of the heart (heart weight 520 g; 180 cm body length, 81 kg body weight) and an asymmetric heart configuration with a hypertrophic right ventricle and round configuration of the apex. The large pulmonary arteries were dilated and showed plaques indicative of pulmonary hypertension.

The manner of death was assessed as a natural death, and the cause of death was determined as right cardiac failure due to PTE.

Discussion

PMCT is widely used and accepted as a complementary examination to forensic autopsy in routine forensic examination [3, 4]. Over the last 10 years, PMMR has been introduced as an additional tool in post-mortem imaging mainly feasible for diagnosis of soft tissue and organ pathology [5, 6]. Acute PTE is a frequently found natural cause of death at autopsy [7]. However, pulmonary infarction accompanying PTE is a less common finding. Pulmonary infarction presents mostly in patients with PTE and reduced cardiac function or pre-existing pulmonary disease. While PTE has been demonstrated in

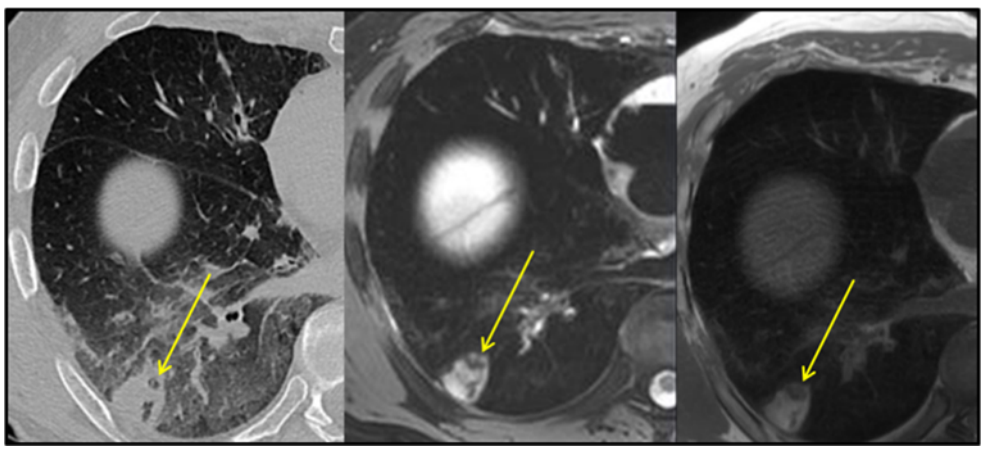

Fig. 1 Axial PMCT (left image), axial in-phase T2w PMMR (middle image), and axial in-phase T1w PMMR (right image) with exemplary wedge-shaped lesion (yellow arrows) in the right lower lobe of the lung

Table 1 Appearance of pulmonary infarction in PMMR in T1w and T2w Dixon sequences

	In-phase	Out-of-phase	Fat only	Water only
T1w	Iso- to hypointense	Iso- to hyperintense	Lesion not visible	Hyperintense
T2w	Iso- to hyperintense	Iso- to hyperintense	Lesion not visible	Hyperintense

PMCT and PMMR [5, 8–12], pulmonary infarction has neither been shown nor discussed in PM-imaging.

Pulmonary infarction may present similarly to other pulmonary findings such as lung cancer and infectious lung disease in CT imaging [13]. In clinical CT, pulmonary infarction is often described as wedge-shaped opacities located at the periphery of the lung [14], also known as "Hampton's hump" [15]. Hyperlucent focal areas may be present within the infarction [16]. Pneumonia, cancerous pulmonary nodules, or septic emboli (Fig. 2) may also appear as pleura-based, wedge-shaped, inhomogeneous lesions in clinical CT [17–19]. Distinction between these entities may therefore be challenging or impossible [13]. Regarding cancerous pulmonary nodules, PMCT is comparable with ante-mortem images in the early post-mortem interval [20]. In our case, we observed wedge-shaped, pleura-based lesions at the lung periphery mainly appearing hyperdense with smaller hypodense areas in PMCT (Fig. 1). Thus, similar appearance of pulmonary infarction in clinical CT and PMCT may be assumed. However, since pulmonary infarction may not be distinguishable from infectious or cancerous lung diseases, PMCT alone may not be enough to strengthen the diagnosis of pulmonary infarction and additional PMMR of the lungs may be useful.

Combined appearance of PTE and wedge-shaped lesions in post-mortem imaging may hint to acute pulmonary infarction. Post-mortem clots in MRI usually show signs of sedimentation due to gravitation with compartments of lower density containing fibrin and compartments with higher density containing erythrocytes. The structure of vital clots like PTE appears homogenous, with intermediate signal intensity on T2w images, in direct contact with the vessel wall and situated within a hypointense layer of sedimented erythrocytes [21]. Older pulmonary infarction may not be accompanied by clear signs of PTE since previous acute PTE may present as strings and webs of connective tissue [22] in the lumen of the pulmonary arteries, or may be completely remnant free. In clinical contrast-enhanced CT-imaging, these strings are connected to the vessel wall on both sides, surrounded by contrast media [23, 24]. As contrast-enhanced imaging is not a routine tool in post-mortem imaging, the diagnosis of chronic PTE will likely be established during autopsy.

Regarding pulmonary infarction, Bray et al. [25] state that appearance of pulmonary infarction in clinical magnetic resonance imaging varies according to the accumulated aging blood within the alveoli and its signal characteristics. Therefore, blood in hyperacute (less than 24 h) pulmonary infarction areas appears hyperintense in T2w and hypointense in T1w whereas the lesions appear hyperintense in T1w in the acute interval (up to 1 week). In the presented case, infarction areas appeared mainly hyperintense with hypointense components in T2w and hypointense to isointense containing small focal hypointense areas in T1w PMMR (Fig. 1). Based on the abovementioned characteristics, this PMMR signal intensity corresponds to an infarction age slightly over 24 h. This is in accordance with the known case circumstances as well as autoptic and histologic findings. It can thus be assumed that in a short post-mortem interval, characteristics of pulmonary infarction in PMMR correspond to those in clinical MRI and may be applied for diagnosis and age determination of pulmonary infarction. Literature regarding pulmonary findings in PMMR is scarce. To the best of our knowledge, there is no literature describing scanning protocols in PMMR for depiction of pulmonary infarction. Some of the faced difficulties in PMMR are rapid changes in signal intensity in a post-mortem interval due to sedimentation, decomposition, and cooling of the corpse [26–28]. Knowing the temperature of the body before scanning is of great importance, as the image contrast decreases for both T1w and T2w images for lower body

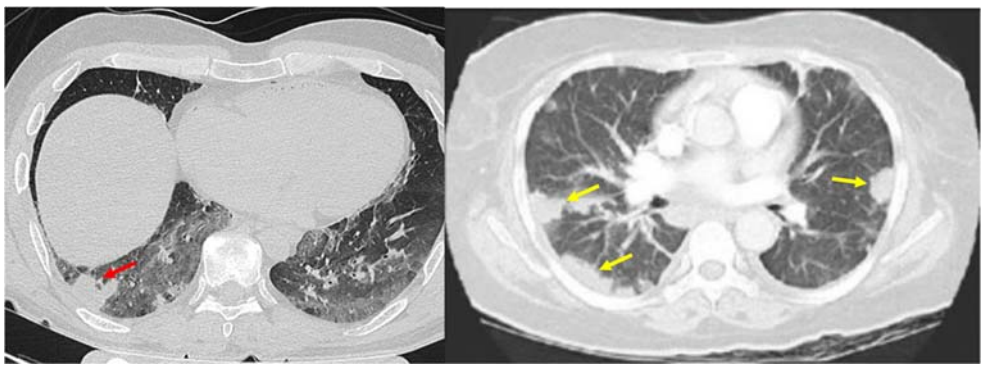

Fig. 2 Depiction of undistinguishable wedge-shaped pleura-based lesions in PMCT and clinical CT. The left image shows unenhanced PMCT with pulmonary infarction (red arrow). The right image shows multiple, pleura-based lesions due to septic emboli (yellow arrows) [19]

temperatures. At a body temperature below 20 °C on T2w and below 10 °C on T1w images, a visible decrease in image contrast was observed [26].

Due to our in-house standard, we used Dixon technique [29] for PMMR imaging. The benefit of Dixon technique lies in the simultaneous generation of fat- and water-suppressed images from a single acquisition. The Dixon in-phase sequences correspond to T1w/T2w images seen in spin-echo sequences. However, fat- and water-suppressed images are not crucial for identification of pulmonary infarctions. Since the appearance of pulmonary infarction in PMMR seems to be similar to clinical MRI, it is mainly dependent on the accumulated blood and its age characteristics. Therefore, conventional T1- and T2-weighted spin-echo sequences will suffice.

Conclusion

Pleura-based wedge-shaped lesions in unenhanced PMCT may indicate pulmonary infarction but lesions may not be distinguishable from other pulmonary pathologies. Additional PMMR of the lungs using conventional T1- and T2-weighted sequences may aid in diagnosis and age determination of pulmonary infarction at a short post-mortem interval.

Compliance with ethical standards This article does not contain any studies with live human participants or animals.

Conflict of interest The authors declare that they have no conflicts of interest.

References

1. Jackowski C, Grabherr S, Schwendener N (2013) Pulmonary thrombembolism as cause of death on unenhanced postmortem 3T MRI. Eur Radiol 23:1266–1270. https://doi.org/10.1007/s00330-012-2728-3
2. (2000) Recommendation no. R (99) 3 of the Committee of Ministers to member states on the harmonization of medico-legal autopsy rules. Forensic Sci Int 111:5–58
3. Willaume T, Farrugia A, Kieffer E-M, Charton J, Geraut A, Berthelon L, Bierry G, Raul JS (2018) The benefits and pitfalls of post-mortem computed tomography in forensic external examination: a retrospective study of 145 cases. Forensic Sci Int 286:70–80. https://doi.org/10.1016/j.forsciint.2018.02.030
4. Mishima S, Suzuki H, Fukunaga T, Nishitani Y (2018) Postmortem computed tomography findings in cases of bath-related death: applicability and limitation in forensic practice. Forensic Sci Int 282:195–203. https://doi.org/10.1016/j.forsciint.2017.11.030
5. Schwendener N, Jackowski C, Persson A, Warntjes MJ, Schuster F, Riva F, Zech WD (2017) Detection and differentiation of early acute and following age stages of myocardial infarction with quantitative post-mortem cardiac 1.5T MR. Forensic Sci Int 270:248–254. https://doi.org/10.1016/j.forsciint.2016.10.014
6. Mokrane F-Z, Savall F, Dercle L, Crubezy E, Telmon N, Rousseau H, Dedouit F (2017) Technical note: a preliminary comparative study between classical and interventional radiological approaches for multi-phase post-mortem CT angiography. Forensic Sci Int 271:23–32. https://doi.org/10.1016/j.forsciint.2016.12.008
7. Micallef MJ (2018) The autopsy and diagnosis of pulmonary thrombo-embolism. Forensic Sci Med Pathol 14:241–243. https://doi.org/10.1007/s12024-018-9950-5
8. Rutty GN, Morgan B, Robinson C et al (2017) Diagnostic accuracy of post-mortem CT with targeted coronary angiography versus autopsy for coroner-requested post-mortem investigations: a prospective, masked, comparison study. Lancet Lond Engl 390:145–154. https://doi.org/10.1016/S0140-6736(17)30333-1
9. Harty MP, Harcke HT, Gould SW, Sukula-Perlman A (2018) Pulmonary embolus as cause of death in an adolescent: demonstration on postmortem CT. Pediatr Radiol 48:745–748. https://doi.org/10.1007/s00247-017-4041-4
10. von Both I, Bruni SG, Herath JC (2018) Differentiation of antemortem pulmonary thromboembolism and postmortem clot with unenhanced MRI: a case report. Forensic Sci Med Pathol 14:95–101. https://doi.org/10.1007/s12024-017-9940-z
11. Ampanozi G, Held U, Ruder TD et al (2016) Pulmonary thromboembolism on unenhanced postmortem computed tomography: feasibility and findings. Leg Med Tokyo Jpn 20:68–74. https://doi.org/10.1016/j.legalmed.2016.04.005
12. Burke MP, Bedford P, Baber Y (2014) Can forensic pathologists diagnose pulmonary thromboembolism on postmortem computed tomography pulmonary angiography? Am J Forensic Med Pathol 35:124–131. https://doi.org/10.1097/PAF.0000000000000086
13. Gaeta M, Ascenti G, Mazziotti S et al (2012) MRI differentiation of pneumonia-like mucinous adenocarcinoma and infectious pneumonia. Eur J Radiol 81:3587–3591. https://doi.org/10.1016/j.ejrad.2011.12.022
14. He H, Stein MW, Zalta B, Haramati LB (2006) Pulmonary infarction: spectrum of findings on multidetector helical CT. J Thorac Imaging 21:1–7. https://doi.org/10.1097/01.rti.0000187433.06762.fb
15. Hampton AO (1940) Correlation of postmortem chest teleroentogenograms with autopsy findings, with special reference to pulmonary embolism and infarction. Am J Roentgenol 43:305–326
16. Miniati M (2016) Pulmonary infarction: an often unrecognized clinical entity. Semin Thromb Hemost 42:865–869. https://doi.org/10.1055/s-0036-1592310
17. Rosado-de-Christenson ML, Abbott GF, McAdams HP, Franks TJ, Galvin JR (2003) From the archives of the AFIP. RadioGraphics 23:759–783. https://doi.org/10.1148/rg.233025165
18. Luciano C, Francesco A, Giovanni V et al (2011) CT signs, patterns and differential diagnosis of solitary fibrous tumors of the pleura. J Thorac Dis 2:21-25–21-25
19. Pictorial essay of radiological features of benign intrathoracic masses. https://www.ncbi.nlm.nih.gov/pmc/articles/PMC4652288/. Accessed 22 Nov 2019
20. Ikeda G, Yamamoto R, Suzuki M, Ishikawa H, Kikuchi K, Shiotani S (2007) Postmortem computed tomography and magnetic resonance imaging in a case of terminal-stage small cell lung cancer: an experience of autopsy imaging in tumor-related death. Radiat Med 25:84–87. https://doi.org/10.1007/s11604-006-0104-4
21. Jackowski C, Thali M, Aghayev E, Yen K, Sonnenschein M, Zwygart K, Dirnhofer R, Vock P (2006) Postmortem imaging of blood and its characteristics using MSCT and MRI. Int J Legal Med 120:233–240. https://doi.org/10.1007/s00414-005-0023-4
22. Pulmonary arterial bands and webs; an unrecognized manifestation of organized pulmonary emboli. https://www.ncbi.nlm.nih.gov/pmc/articles/PMC1949576/. Accessed 14 Nov 2019
23. Castañer E, Gallardo X, Ballesteros E et al (2009) CT diagnosis of chronic pulmonary thromboembolism. RadioGraphics 29:31–50. https://doi.org/10.1148/rg.291085061

24. Chronic pulmonary embolism: diagnosis. https://www.ncbi.nlm.nih.gov/pmc/articles/PMC6039808/. Accessed 14 Nov 2019
25. Bray TJP, Mortensen KH, Gopalan D (2014) Multimodality imaging of pulmonary infarction. Eur J Radiol 83:2240–2254. https://doi.org/10.1016/j.ejrad.2014.07.016
26. Ruder TD, Hatch GM, Siegenthaler L, Ampanozi G, Mathier S, Thali MJ, Weber OM (2012) The influence of body temperature on image contrast in post mortem MRI. Eur J Radiol 81:1366–1370. https://doi.org/10.1016/j.ejrad.2011.02.062
27. Ruder TD, Thali MJ, Hatch GM (2014) Essentials of forensic post-mortem MR imaging in adults. Br J Radiol 87. https://doi.org/10.1259/bjr.20130567
28. Wagensveld IM, Blokker BM, Wielopolski PA et al (2017) Total-body CT and MR features of postmortem change in in-hospital deaths. PLoS One 12. https://doi.org/10.1371/journal.pone.0185115
29. Dixon WT (1984) Simple proton spectroscopic imaging. Radiology 153:189–194. https://doi.org/10.1148/radiology.153.1.6089263